Metallography, Microstructure, and Analysis (2023) 12:26–33
https://doi.org/10.1007/s13632-023-00928-4

PEER-REVIEWED PAPER

Microstructure and Mechanical Properties of Hot Pressed Oxide Dispersion Strengthened NITRONIC-60 Austenitic Stainless Steels Developed Through Mechanical Alloying

R. Mariappan[1] · J. Chandradass[2] · M. Murali[1]

Received: 6 November 2022 / Revised: 15 January 2023 / Accepted: 19 January 2023 / Published online: 13 February 2023

Abstract

In the present study, three different steels were developed from water atomized pre-alloyed powder such as N60 (17Cr-8Mn-4Si), MM-N60 (Mechanical Milled 17Cr-8Mn-4Si) and MM-N60-Y (Mechanical Milled 17Cr-8Mn-4Si-0.3Y_2O_3) with and without addition of Yttria. MM-N60 and MM-N60-Y were mechanically milled under high energy ball mill for the period of 2, 4, 6, 8 and 10 h to obtain nanocrystallite structure followed by hot pressing at the temperature of 1250 ± 10 °C with a pressure level of 56 MPa. For comparison, the un-milled powder was also consolidated into a bulk sample under the same processing condition. The microstructure of all three hot-pressed samples was examined under optical, scanning electron, and transmission electron microscopes. Using a Hounsfield tensometer and Vicker's microhardness tester, the mechanical characteristics of these samples were assessed. The grain size of hot pressed samples from the milled powders is lesser than the compact of the un-milled powder. The Y_2O_3 added austenitic stainless steel (MM-N60-Y) shows the least austenite grains size around 2.8 µm compared to MM-N60 (without Y_2O_3). Such a highly refined austenitic grain with Y_2O_3 dispersoid resulted in the highest hardness, yield, and tensile strength among the three samples. The tensile strength of as high as 758 MPa and a hardness of 484 VHN were obtained in the nano-Y_2O_3 dispersed ODS austenitic alloy.

Keywords Austenitic stainless steel · Oxide dispersion strengthening · Mechanical milling · Micro-structure · Tensile strength

Introduction

Nitrogen hardened 17Cr/4Ni (Nitronic-60) is austenitic stainless steel (AS) known for its exceptional wear and abrasion resistance. Marine shafts, automobile valves, and fasteners are some of the typical applications for this grade of steel [1–3]. The mixed oxides film of Cr_2O_3 and SiO_2 forms on the surface of this steel with the nominal composition of Fe-17Cr-8Mn-8.5Ni-4Si-0.14N-0.1C, which is stabilized by the nitrogen dissolved in the matrix, impart good high-temperature corrosion resistance [4, 5]. Due to the presence of high ferrite stabilizers like Cr and Si in the austenitic matrix, delta ferrite can sometimes form in the single-phase austenitic structure of this steel. The delta ferrite precipitates can inhibit grain growth and thus improves the alloy's strength [6–8]. The nitrogen dissolved in the austenitic matrix also dramatically increases the strength. The production of brittle stable nitrides and intermetallic precipitates due to sluggish cooling of ingot casting severely restricts the scope of nitrogen's use for strengthening.

Powder metallurgy (PM) processing is one of the effective ways of overcoming the limitations associated with high nitrogen steels [6, 9]. In nitrogen-alloyed steel, the PM method proved favorable due to its homogenous distribution, increased nitrogen content due to the quick solidification of powder particles during atomization, and nitrogen content control. By using the PM method, the addition of nitrogen up to 0.6% demonstrating good strength and ductility has been shown in this steel [4, 10]. Components with complex shapes, difficult to manufacture by casting,

✉ R. Mariappan
mariappanmukund@gmail.com

✉ J. Chandradass
chandraj@srmist.edu.in

1 Department of Physics, Saranathan College of Engineering, Trichy 620012, India

2 Centre for Automotive Materials, Department of Automobile Engineering, SRMIST, Chengalpattu 603203, India

and thermo-mechanical processes can be produced using the various near-net shaping techniques. The dispersion of nano-sized oxides in the austenite grains can further enhance the Nitronic-60 steel's high-temperature strength, hardness, and wear resistance. Several researchers established the approach's effectiveness in ferritic stainless steels [4, 5]. The nano-size oxide particles prevent grain coarsening and arrest the movement of dislocations at elevated temperatures by the Zener pinning effect, which eventually increases the creep resistance [6]. Because of the enhanced particle strengthening effects resulting from the Orowan mechanism, these nano-sized oxide dispersion strengthened (ODS) alloys have superior mechanical properties to micron-sized ODS alloys with same volume content. [7]. Investigation of the effects of oxide nanoparticles dispersion in the austenitic stainless steel, in particular, 17Cr/4Si steel, is not yet reported.

The effect of nanoscale oxides on the microstructure and mechanical characteristics of the austenitic stainless steel 17Cr/4Si were examined. Mechanical milling and vacuum hot pressing are used to consolidate the pre-alloyed powders with (MM-N60-Y) and without the Y_2O_3 addition (MM-N60) into bulk samples under the same conditions. Evaluations and comparisons were made between the samples' densification, microstructure, and mechanical characteristics and those made by directly pressing the pre-alloyed powder.

Experimental Procedure

Powdered 17Cr/4 Si (Nitronic-60) austenitic stainless steel was employed in this investigation, and its chemical composition is listed in Table 1. The pre-alloyed austenitic stainless steel powder (referred to as N60) (Sandvik Pvt. Ltd, Sweden) was mechanically milled in a planetary ball mill (Fristch Pulverisette 7, Germany) with and without adding 0.3 wt.% Y_2O_3 (Alfa Aesar, USA). The powder was milled at a ball-to-powder ratio of 10:1 in a pair of WC–Co vials at 300 rpm for 2–10 h in a toluene medium. Particle size and its distribution were analyzed by using the laser diffraction technique (Malvern Instruments Limited, UK). Further, the powder morphologies were also assessed with scanning electron microscopy (Hitachi, Tokyo, Japan). The mechanically milled N60 powders without Y2O3 addition (MM-N60) and with 0.3 wt.% Y2O3 addition (MM-N60-Y) and un-milled starting powder (N60) were consolidated by hot pressing at 1250 °C and under 56 MPa pressure in a 10–3 mbar vacuum atmosphere for 90 min. After hot pressing, the samples were cooled at 30 degrees per minute. Archimedes' method was applied to determine the density of the consolidated samples. The relative density (ρ_r) was calculated using the theoretical density (ρ_{th}) given by the supplier for N60 and MM-N60 samples. The MM-N60-Y sample was estimated from the density of N60 and Y_2O_3 using the simple rule of mixtures. An optical microscope and SEM combined with energy dispersive spectroscopy were used to analyze the microstructure of hot-pressed materials (EDS). Transmission electron microscopy (TEM—INCA Sight- JEOL, JEM-2100) at 200 kV is used to examine the MM-N60-Y sample's finer details. Ion milling was done after dimpling grinding (Gatan Model 656) to prepare the TEM samples (Precision ion polishing system-Gatan Model 691). After polishing the samples to a mirror finish, the hardness of the hot-pressed samples was assessed using a Vickers micro-hardness tester with a 1 kg load and a 15 s dwell period. The hardness values reported are the average of ten readings taken at different locations in each sample. The Hounsfield Tensometer (Kundale India Ltd, India) was used to test the tensile qualities of the hot-pressed samples in accordance with the ASTM-E8 standard.

Results and Discussion

Powder Preparation and Consolidation

SEM pictures of N60, Y_2O_3 powders and mechanically milled N60-0.3Y_2O_3 (MM-N60-Y) for 5 h and 10 h are shown in Fig. 1a–d. The N60 powder was spherical with a mean particle size of 3 µm, and the Y_2O_3 powder was irregular in shape with a mean particle size of 1 µm. Upon mechanical milling, the fracturing and welding between the particles resulted in spherical and irregular-shaped particles, as shown in Fig. 1c and d after 5 and 10 h milling. The particle size of the 10 h milled N60 and N60-Y powders are 18 nm and 12 nm, respectively. The Debye-Scherer formula has been used to determine the crystallite size of the milled powder. The structural evolution during mechanical milling of the N60 and N60 mixed with 0.3 wt.% Y_2O_3 powder was analyzed using XRD. Since the XRD patterns of MM-N60 powder and MM-N60-Y are identical, the XRD

Table 1 Chemical composition of the three austenitic stainless steel powder

Alloy	Element concentration (wt.%)							
	C	Cr	Ni	Si	Mn	N	Y_2O_3	Fe
N60	0.1	17	8	4	9	0.1	Nil	Bal
MM-N60	0.1	17	8	4	9	0.1	Nil	Bal
MM-N60-Y	0.1	17	8	4	9	0.1	0.3	Bal

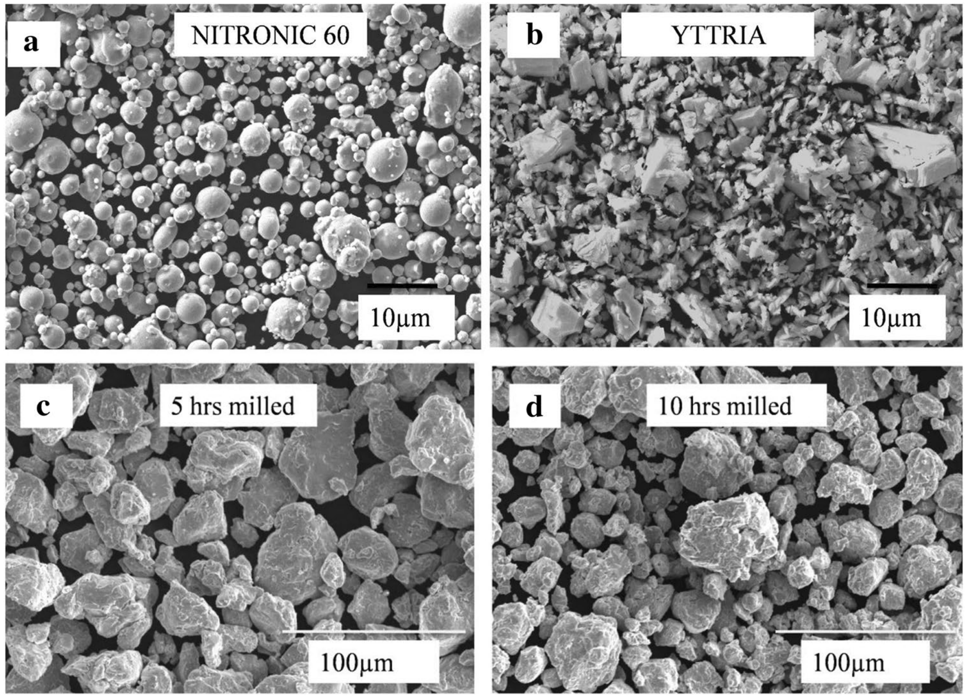

Fig. 1 SEM morphology of (**a**) Nitronic-60 (N60); (**b**) yttrium oxide powder; (**c**) MM-N60-Y milled for 5 h and (**d**) for 10 h

Table 2 Relative densities of the hot pressed N60, MM-N60, and MM-N60-Y compacts

S No	Samples	Relative density
1	N60	95.8
2	MM-N60	97.6
3	MM-N60-Y	96.9

pattern of MM-N60-Y has only been presented in this discussion. Since the nitronic 60 steel powder is a special alloy powder, unmilled powder has shown dual peaks of austenite and ferrite. Even though N60 is monophasic stainless steel, the presence of ferrite stabilizer silicon and chromium in the steel could stabilize the alpha phase along with gamma phases.

When the milling time increases, dual peaks are diminished, and a single austenitic peak has been formed. The XRD pattern shows only peaks corresponding to the austenite (γ) phase though the presence of traces of ferrite (α) cannot be ruled out. Due to their reduced presence in the present composition, the XRD patterns could not identify the Y_2O_3 diffraction peaks [10]. The substantial broadening of the d_{hkl} ($2\theta = 43°$) in the 10 h milled powder confirms that the crystallite size of the MM-N60-Y powder was reduced to 12 nm. Similarly, a crystallite size of 18 nm was exhibited for 10 h of milled MM-N60 powder.

Table 2 gives the relative density of the hot press consolidated N60, 10 h mechanically milled N60 (MM-N60), and N60 mixed with 0.3 wt.% Y_2O_3 (MM-N60-Y) samples.

All the samples show density > 95%, indicating they reached the final sintering stage, having only isolated pores. The relative density differences between the samples are less than 2%. Compact prepared from MM-N60 has exhibited the highest density among them. Both the milled powders MM-N60 and MM-N60-Y showed relatively higher densities than unmilled base powder (N60), which is expected as the milled powders likely have more structural defects, and favor faster diffusion of atoms during hot pressing. Moreover, the finer crystallite and particle size in the milled powder, which will result in a very high volume of grain boundaries and specific surface area, can also increase the driving force for densification. The addition of Y_2O_3 tends to reduce the sintering kinetics marginally (Fig. 2).

Microstructural Examination of Consolidated Samples

The optical micrographs of the hot-pressed N60, MM-N60, and MM-N60-Y samples are shown in Fig. 3. The microstructure of the N60 sample shows large equiaxed austenitic grains with an average size of 18 μm. However, in MM-N60 and MM-N60-Y samples, the austenite grain sizes are fine and not visible in a low magnification optical microscope. The 10 h ball milling carried out in the MM-N60 and MM-N60-Y powder substantially reduces the grain sizes of both AS powder and Y_2O_3. Apart from improving the densification, as explained in the previous section, such fine structures resulted in very fine austenitic grains in the consolidated samples. The ASTM (Jefrrie's Planimetric) method

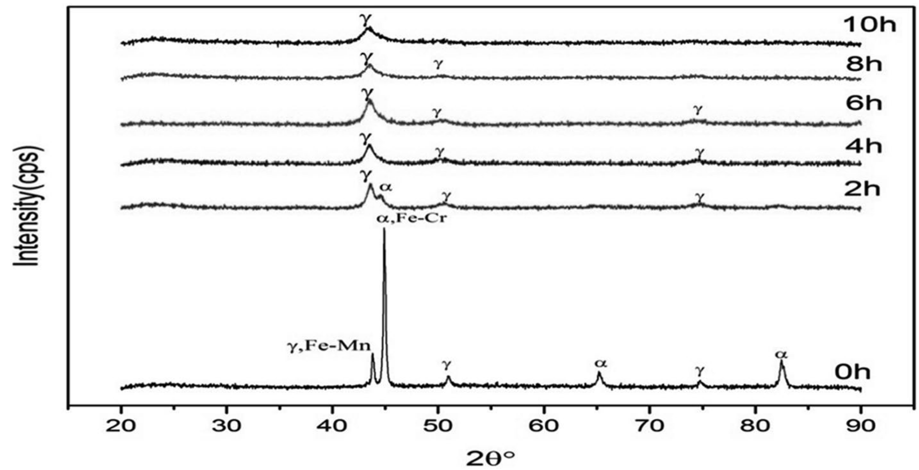

Fig. 2 XRD patterns of mechanically alloyed MM-N60-Y powder

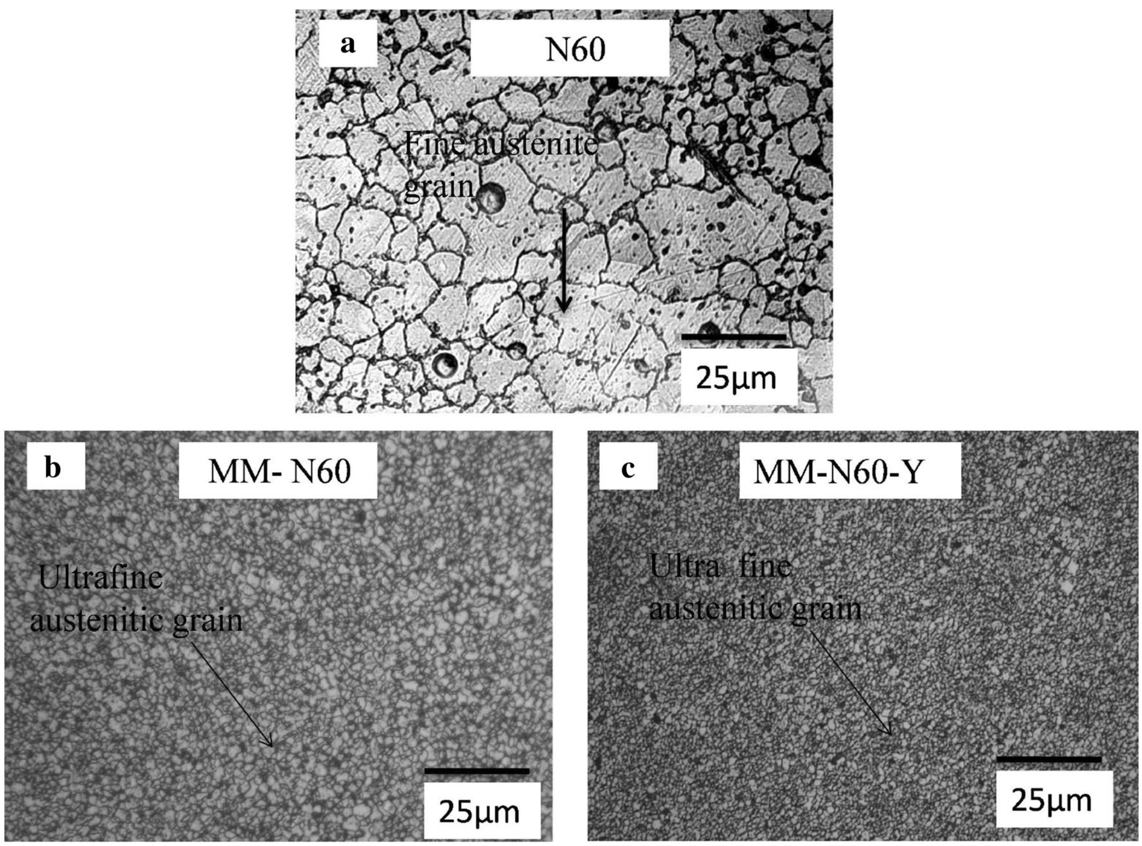

Fig. 3 Microstructure of (**a**) N60 (**b**) MM-N60 and (**c**) MM-N60-Y AS hot-pressed compacts

was used to measure the grain size of the hot-pressed AS samples, and the results are shown in Table 3. The grain sizes were measured from SEM micrographs taken at 2000 X magnification. The samples from mechanically milled MM-N60 and MM-N60-Y powder showed grain sizes one order lesser than the unmilled N60 sample. MM-N60-Y power has an average grain size of 2.8 µm, which is 1.43 times more refined than the MM-N60 powder (average grain

Table 3 Hot-pressed AS compacts' ASTM grain size and average grain size

Composition	ASTM grain size number	Average grain diameter, µm
N60	2	18
MM-N60	13	4
MM-N60-Y	14	2.8

size of 4 μm), suggesting that the Y_2O_3 in the milled powder act as a grain growth inhibitor during densification.

Figure 4 shows SEM and EDS investigation of the hot pressed MM-N60 sample on grain and at the austenitic grain boundary. Figure 4 shows that the grain mainly comprises austenitic stabilizing elements like nickel and manganese. This shows that the existing phase is austenite. Similarly, EDS analysis at the interfaces of austenitic grain (Fig. 4b) consists of higher chromium content and lower nickel content relatively within the grain structure, as is evident from Table 3. However, chromium concentration at the interface has not exceeded the critical limit, which means that small dark precipitates observed at the interfaces are delta ferrite. However, a good amount of Fe (approximately 63 percent) content was also observed at the interfaces, confirming ferrite stabilization.

Many researchers reported that delta ferrite and chromium-rich precipitate formation depends on the cooling rate after the heat treated above 1000 °C. Nitronic-60 steel, heat treated at 1020 °C followed by water quenching, showed delta ferrite and austenite. However, the formation of chromium-rich precipitates was observed in the steel annealed between 400 and 850 °C [11–13]. The delta ferrite, sigma phase, austenitic phase, and amorphous silica were formed in the stainless steel heat treated in the CO/H_2 mixture environment at 650 °C [14]. The stainless steel was processed at a temperature of 1250 °C with a cooling rate of 25–30 °C per minute, which is significantly over the critical cooling rate for the development of chromium-rich precipitates in powder metallurgy-prepared stainless steel [15, 16].

Table 4 shows the elemental composition of the hot pressed MM-N60 billets as obtained from the EDS analysis. From Table 2, it is clear that the grain and grain boundary contain appropriate composition of austenite and ferrite. On the other hand, the grains were found to contain an optimum content of chromium, nickel and manganese, which stabilized the austenitic phase.

Figure 5a, b shows the TEM micrograph of the hot pressed MM-N60-Y sample. The matrix consists of austenite grain, and fine dispersoids are seen in the micrograph. Oxide

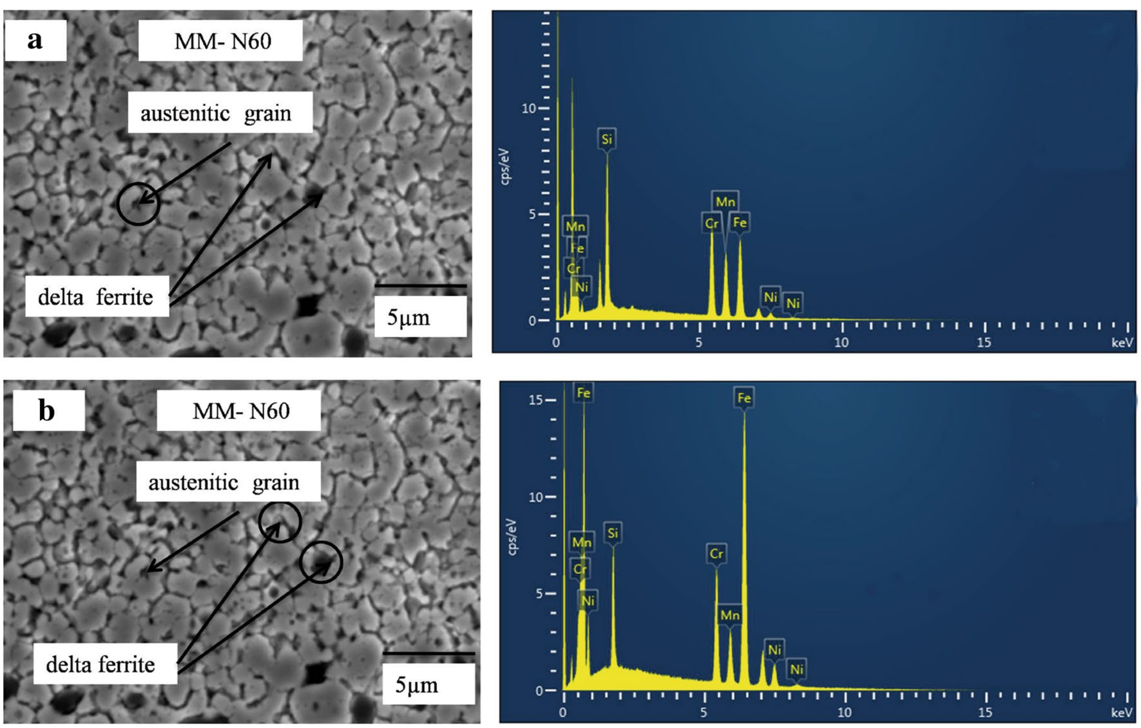

Fig. 4 SEM EDS analysis of MM N60 sample (**a**) on austenite grain and (**b**) along the grain boundary

Table 4 Chemical examination of hot-pressed stainless steel billet grains and boundaries

Composition	Elemental concentration, wt%					
	Phase	Cr	Ni	Mn	Si	Fe
MM-N60	Grain	16.1	9.0	8.6	3.9	Bal
	Grain Interface	22.0	6.9	7.5	4.3	Bal

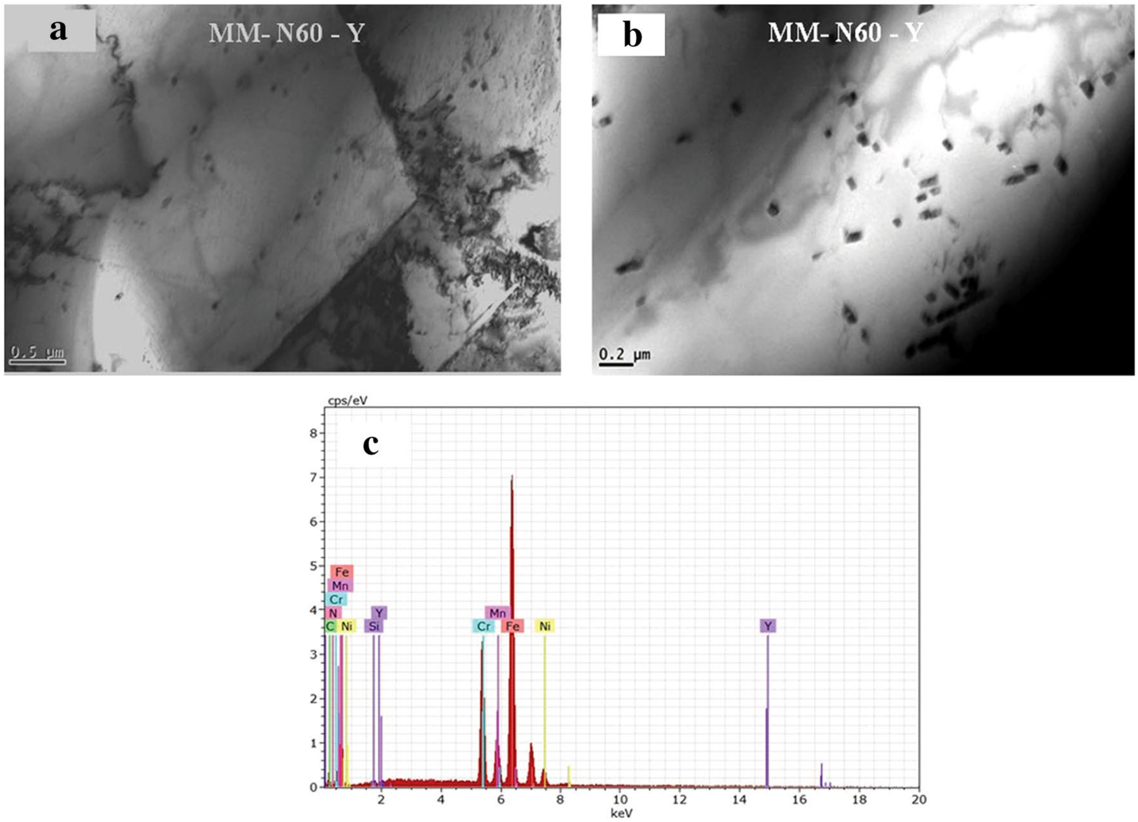

Fig. 5 TEM Micrograph of MM- N60-Y (**a**) austenite grain, (**b**) fine dispersoids along the Austenitic matrix and (**c**) EDS analysis of MM-N60-Y

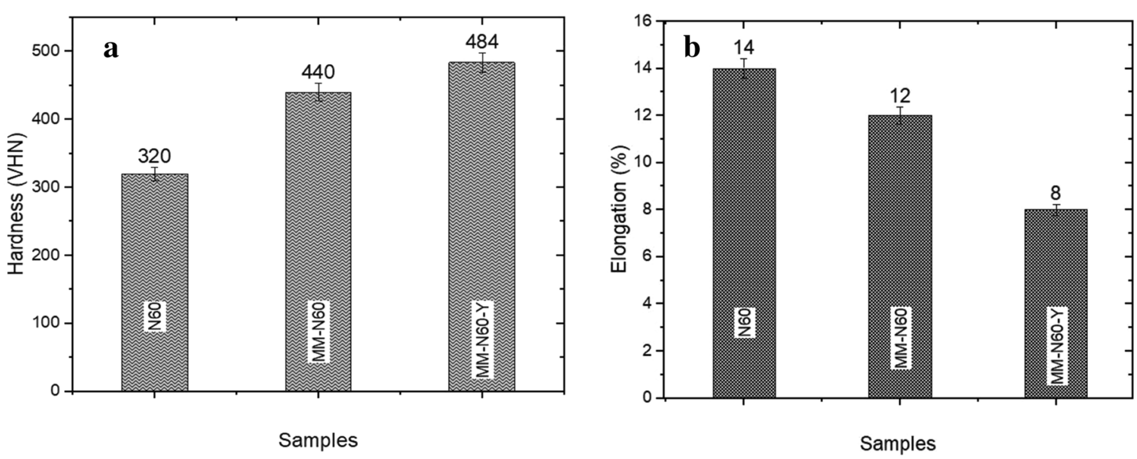

Fig. 6 (**a**) Micro-hardness, (**b**) Elongation of hot pressed N60, MM-N60 and MM-N60-Ysteels

dispersed particle size, number density, uniform distribution, and structure are crucial to mechanical characteristics [17]. The average dispersoid size of approximately 30 nm is uniformly distributed along the austenitic matrix. Recent research shows that the fine spherical dispersoids are pinning the slipping dislocations, which arrest the dislocation movement [18] to improve mechanical properties. EDS analysis of fine dispersoids along with the matrix elements is shown in Fig. 5c.

Mechanical Properties of Hot Pressed Samples

Microhardness, percent elongation, yield strength, and ultimate tensile strength of hot-pressed N60, MM-N60, and MM-N60-Y are shown in Figs. 6 and 7. Mechanically milled samples have higher hardness, yield strength, and tensile strength than the basic alloy. The Y_2O_3 dispersed MM-N60-Y sample showed the highest hardness and yield strength. The effect of the difference in densities in the samples over their mechanical properties is likely marginal. As mentioned earlier, the difference is less than 2%. The ultrafine grain size of the austenitic phase was principally responsible for the greater hardness and strength in MM samples. The Y_2O_3 nano dispersoid in the austenitic grains also benefits the steel by improving the hardness and strength. This is demonstrated by the strength determined from the austenite grain size using the Hall–Petch relation: $\sigma_y = \sigma_o + kd^{-1/2}$ where σ_y is yield strength in MPa, σ_o is intrinsic friction stress (Peierls stress) in MPa, k is a constant (Hall–Petch coefficient, MPa/m$^{1/2}$) that represents the inhibition of the grain boundary to deformation, and d is the grain size [19]. The yield strength calculated for the MM-N60 sample of 4 μm grain size is 584 MPa which is around 12% lesser than the 666 MPa measured in the MM-N60-Y sample. Hence, the higher strength of MM-N60-Y is due to the contribution of fine austenitic grains and the nano Y_2O_3 dispersoid. The percentage elongation indicates the deformability of the alloy affected by the Y_2O_3 dispersion. Fracture morphologies of N60, MM-N60, and MM-N60-Y of the steels are shown in Fig. 8a, b, and c, respectively. Figure 8a is dimples of varying sizes from larger to smaller, in contradictory mechanically milled yttria added to steel (MM-N60-Y) very fine dimples along with micro-crack and micro-pores. Hence, MM-N60-Y steel has undergone the least ductile failure mode compared with the other two stainless steels. From these results, it is clear that yttria-added steel (MM-N60-Y) has high strength and less ductile nature due to the austenitic grain refinement along with second phase oxide dispersion strengthened particles [20, 21]. However, mechanically milled MM-N60 steel has a finer size of dimples compared with unmilled N60 steel. These failure modes of N60 and MM-N60 samples have undergone completely ductile fracture, which is evident from the percent elongation.

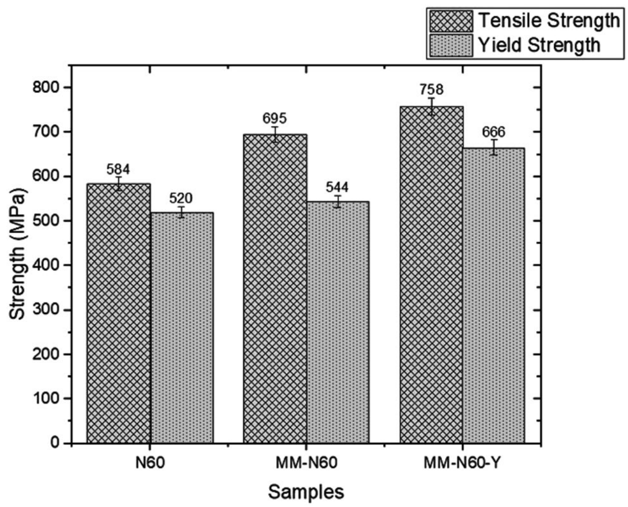

Fig. 7 Strength of hot pressed N60, MM-N60 and MM-N60-Y AS

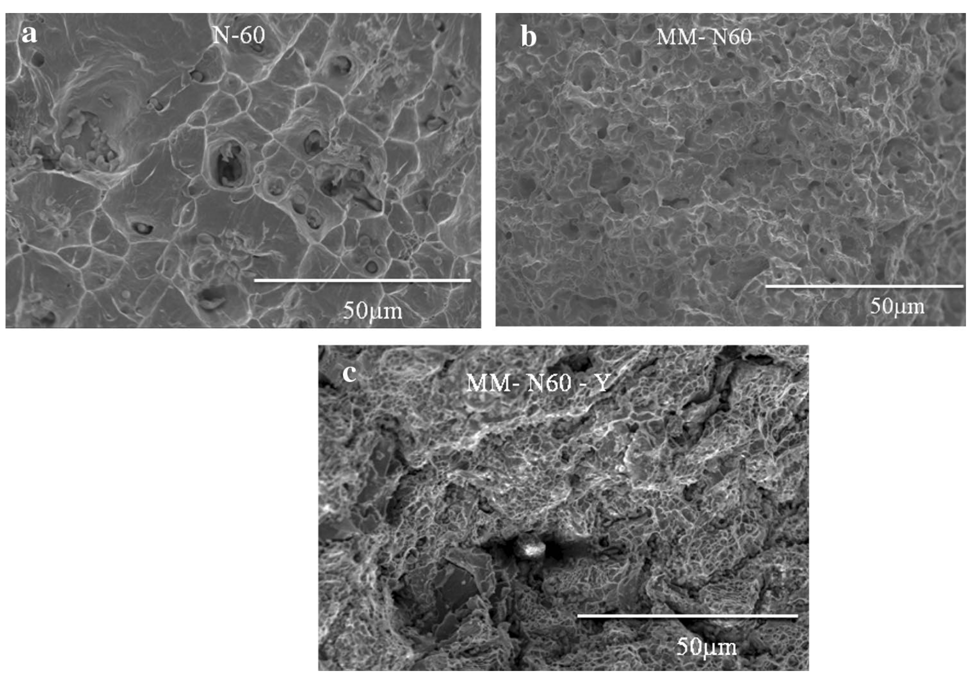

Fig. 8 Fracture morphologies of (**a**) N60, (**b**) MM-N60 and (**c**) MM-N60-Y steels

Conclusions

Yttria-added oxide dispersion strengthened NITRONIC-60 steel has been developed through mechanical milling followed by the hot pressing method.

The following results are

- Mechanically milling of MM-N60 powder resulted in significant grain size reduction in the consolidated samples. The addition of Y_2O_3 (MM-N60-Y) also inhibits austenite grain growth by Zener pinning.
- Y_2O_3 addition and mechanical milling improve the hardness, yield strength, and tensile strength of the N60 steel. The fine uniformly dispersed nano-sized Y_2O_3 in the equiaxed austenite grain resulted in maximum tensile strength of 758 MPa and a hardness of 484 VHN in this steel.

Acknowledgements The authors would like to express their gratitude to Dr. S. Ravindran, Secretary of Saranathan College of Engineering, Trichy, for granting permission to publish the paper. The authors are grateful to the Department of Science and Technology (No. DST/TSG/NTS/2013/03-G) for sponsoring the project under the Technology Development Programme. The author would also like to thank RANE Engine Valve Limited, Chennai, for working on the project and providing SEM-EDS lab facilities. The authors would like to thank M/s. SANDVIK for providing the powdered Nitronic-60 stainless steel.

References

1. I. Shibahara, S. Ukai, S. Onose, S. Shikakura, Irradiation performance of modified 316 stainless steel for Monju fuel. J. Nucl. Mater. **204**, 131–140 (1993)
2. F. Masuyama, History of power plants and progress in heat resistant steels. ISIJ Int. **41**(6), 612–625 (2001)
3. T. Sourmail, Precipitation in creep resistant austenitic stainless steels. Mater. Sci. Technol. **17**(1), 1–14 (2001)
4. C. Suryanarayana, Mechanical alloying and milling. Prog. Mater Sci. **46**(1–2), 1–184 (2001)
5. S. Ukai, M. Fujiwara, Perspective of ODS alloys application in nuclear environments. J. Nucl. Mater. **307**, 749–757 (2002)
6. J. Rösler, M. Bäker, H. Harders, Mechanical behaviour of metals. In Mechanical Behaviour of Engineering Materials. pp. 165–225. Springer (2007)
7. M.K. Lee, J.J. Park, C.K. Rhee, Synthesis and structural properties of Ni–20Cr–2Y2O3 nanocomposite alloy prepared by a very high energy mechanical milling. Mater. Chem. Phys. **137**(1), 129–134 (2012)
8. M. Wang, H. Sun, L. Zou, G. Zhang, S. Li, Z. Zhou, Structural evolution of oxide dispersion strengthened austenitic powders during mechanical alloying and subsequent consolidation. Powder Technol. **272**, 309–315 (2015)
9. P. Susila, D. Sturm, M. Heilmaier, B.S. Murty, V.S. Sarma, Microstructural studies on nanocrystalline oxide dispersion strengthened austenitic (Fe–18Cr–8Ni–2W–0.25 Y2O3) alloy synthesized by high energy ball milling and vacuum hot pressing. J. Mater. Sci. **45**(17), 4858–4865 (2010)
10. M.P. Phaniraj, D.I. Kim, J.H. Shim, Y.W. Cho, Microstructure development in mechanically alloyed yttria dispersed austenitic steels. Acta Mater. **57**(6), 1856–1864 (2009)
11. L. Chen, X. Ma, L. Wang, X. Ye, Effect of rare earth element yttrium addition on microstructures and properties of a 21Cr–11Ni austenitic heat-resistant stainless steel. Mater. Des. **32**(4), 2206–2212 (2011)
12. J.H. Magee, Jr., Galling resistant austenitic stainless steel alloy. In: Google Patents (1989).
13. A. Gigovic-Gekic, M. Oruc, A. Nagode, H. Avdusinovic, Effect of heat treatment and test temperature on fracture type of steel Nitronic 60 Vpliv toplotne obdelave in temperature preizkušanja na vrsto preloma jekla Nitronic 60. RMZ Mater. Geoenviron. **58**(2), 121–128 (2011)
14. Y. Miao, K. Mo, B. Cui, W.-Y. Chen, M.K. Miller, K.A. Powers, V. McCreary, D. Gross, J. Almer, I.M. Robertson, J.F. Stubbins, The interfacial orientation relationship of oxide nanoparticles in a hafnium-containing oxide dispersion-strengthened austenitic stainless steel. Mater. Charact. **101**, 136–143 (2015)
15. F. Martín, C. García, Y. Blanco, M. Rodriguez-Mendez, Influence of sinter-cooling rate on the mechanical properties of powder metallurgy austenitic, ferritic, and duplex stainless steels sintered in vacuum. Mater. Sci. Eng., A. **642**, 360–365 (2015)
16. C. Munez, M. Utrilla, A. Urena, Effect of temperature on sintered austeno-ferritic stainless steel microstructure. J. Alloy. Compd. **463**(1–2), 552–558 (2008)
17. I. Hilger, X. Boulnat, J. Hoffmann, C. Testani, F. Bergner, Y.D. Carlan, F. Ferraro, A. Ulbricht, 'Fabrication and characterization of oxide dispersion strengthened (ODS) 14Cr steels consolidated by means of hot isostatic pressing, hot extrusion and spark plasma sintering. J. Nucl. Mater. **472**, 206–214 (2016)
18. Y. Peng, L. Yua, Y. Liua, Z. Ma, H. Li, C. Liu, J. Wu, Microstructures and tensile properties of an austenitic ODS heat resistance steel. Mater. Sci. Eng. A. **767**, 138419 (2019)
19. S. Ganesh, P. Sai-Karthik, M. Ramakrishna, A.V. Reddy, S.B. Chandrasekhar, R. Vijay, Ultra–high strength oxide dispersion strengthened austenitic steel. Mater. Sci. Eng. A. **814**, 141192 (2021)
20. Z. Zhou, S. Sun, L. Zou, Y. Schneider, S. Schmauder, M.W.Z. Zhoua, S. Sun, L. Zou, Y. Schneider, S. Schmauder, M. Wang, Enhanced strength and high temperature resistance of 25Cr20Ni ODS austenitic alloy through thermo-mechanical treatment and addition of Mo. Fusion Eng. Des. **138**, 175–182 (2019)
21. R. Zhuo, H. Jia, S. Cao, Z. Tong, Z. Zhou, Effect of the addition Y and Y_2O_3 on microstructure and mechanical properties of 15cr-15Ni ODS steels. Nucl. Mater. Energy. **31**, 101196 (2022)

Publisher's Note Springer Nature remains neutral with regard to jurisdictional claims in published maps and institutional affiliations.